Electrochemical assessment of high active area of cobalt deposited in deep eutectic solvent

Albert Serrà[1,2], Paula Sebastián[3,*], Midori Landa-Castro[1,4], Elvira Gómez[1,2]

[1] Departament de Ciència de Materials i Química Física, Universitat de Barcelona, Martí i Franquès, 1, 08028 Barcelona, Spain.

[2] Institute of Nanoscience and Nanotechnology (IN^{2}UB), Universitat de Barcelona, Barcelona, Spain.

[3] Department of Chemistry, University of Copenhagen, Universitetsparken 5, 2100 Copenhagen, Denmark

[4] Universidad Autónoma Metropolitana-Azcapotzalco, Departamento de Materiales, Av. San Pablo 180 Col, México

Corresponding author: (paula.sebastian25@gmail.com)

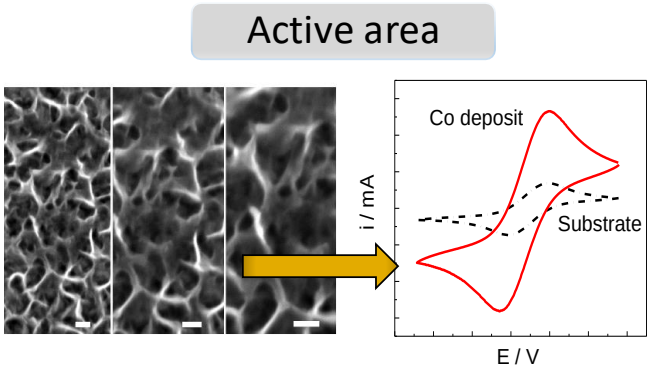

Graphical Abstract

Abstract

Preparation of nanostructured materials with highly efficient active area is crucial for advancement in fields of electrocatalytic conversion of energy, energy storage, or biomedicine. In this regard, there are two main challenges in the electrochemical preparation of high-extended surface area of the nanostructures: 1) establishing the optimal potential conditions to enhance the active area while reducing the size of the prepared material and, 2) simultaneously, finding a practice and simple *in situ* methodology to qualitatively test the increase in the active surface area. Herein, we investigate the cobalt electrodeposition in choline chloride plus urea deep eutectic solvent (DES) and the effect of the DES in the increase of the active surface area of deposited Co films. *In situ* classical electrochemical techniques, in combination with *ex situ* characterization techniques, were employed to establish the best potential conditions to obtain metallic Co films with high active surface area. Then, the increase in active area was tested by using different voltammetric methodologies. The increase in intensity of the outer sphere electron transfer was tested as a tool to analyze the superficial change after cobalt deposition. Voltammetric response in organic medium using benzoquinone on Co films and in an aqueous medium using $Ru(NH_3)_6$, after covering the Co films with gold via galvanic displacement, was assessed. Later, as alternative method, the active area of the freshly deposited Co films, after superficial modification with Au, was tested by lead underpotential deposition. Lead underpotential deposition on gold is a surface-structure process that indirectly allows the estimation of the increment in active area of prepared Co films.

Keywords

Co electrodeposition, deep eutectic solvent, surface active area, outer sphere electron probes, lead underpotential deposition.

1. Introduction

Functionalization of substrates to increase its performance in different electrochemical applications, such as electrocatalysis, energy storage, biosensors, or bioelectrochemistry, is an expanding topic [1–4]. For the majority of the applications, the main interest is focused on the enhancement of effective area versus geometrical one, as well as the intrinsic properties of the material. This is especially relevant when the final application of the material is to be an effective carrier or the miniaturization of the size of the dispositive while keeping high surface area [5–8]. Cobalt, in particular, has magnetic properties that opens the possibility to drive a dispositive under a magnetic field. Furthermore, materials containing cobalt have been observed to allow the adsorption of some active principles, used to carry out reactant functionalizators. This is particularly interesting to develop drug delivery nanotechnology or micro/nanomotors for water treatment applications [1,5,9–11].

Because of the interesting magnetic, chemical, and electrochemical properties of Co, finding more affordable and sustainable strategies for the synthesis of Co materials is necessary for further scaling of the preparation methods. Electrodeposition of Co based materials in DES, under potentiostatic conditions, was previously demonstrated to be a valuable method for tailoring both morphology and chemical composition of deposited cobalt species, by simply tuning the applied potential [5,7,9,12,13]. This would be particularly useful for the preparation, in a controlled way, of preferred deposits for different electrocatalytic applications [5]. In contrast, electrodeposition of Co in aqueous solution is substantially more difficult due to the higher electrocatalytic activity of the cobalt towards the reduction of protons and water, i.e., the hydrogen evolution reaction (HER) [14–17]. The HER overlaps with the deposition process which increases the porosity and negatively affects the quality and uniformity of the Co film. This makes the

deposition of cobalt in a simple aqueous bath extremely difficult unless a variety of additives are used to stabilize the deposition process [14–17]. Deposition of Co in DES, on the other hand, does not require the use of additives or surfactant agents. Notably, deposits under moderately applied overpotentials provide magnetic metallic cobalt in the DES medium, to be used, as abovementioned, in functionalized nanomaterials driven by a magnetic field [6,9,18,19].

Considering that miniaturization is a goal in almost any application, the simultaneous increase of effective surface area is also a challenge, especially in those applications where the carrier function is sought. Under these circumstances, to reduce loading of the metal is also an important parameter. This work has a double pursuit: 1) attaining the cobalt deposition at conditions at which electroactive or effective area is enhanced and 2) simultaneously finding a practice and simple *in situ* methodology to qualitatively evaluate the increase of active surface area. In order to fulfill these two goals, we started assessing the most optimal potential window to prepare nanostructured metallic Co deposits in DES with high surface area and on different substrates, aiming to functionalize different types of materials. Glassy carbon and silicon covered with seeds of Ti and Au were selected as substrates for the Co deposition. Classical electrochemical techniques used to stablish the adequate potential conditions were employed in combination with scanning electron microscopy, X-ray photoelectron microscopy and X-ray diffraction to evaluate the morphology and chemical composition of obtained deposits. Then, the active area of deposited Co films, deposited on Au films, were assessed using different voltammetric methods. For some of them, previously, Co films were covered by gold via a galvanic displacement reaction. This was made to protect the Co from being oxidized during some of the voltammetric analysis of the surface active area. Outer sphere reaction probes and underpotential deposition (UPD) of lead were examined to test the change in active area

of Co films. Outer sphere electron transfer of different redox pairs and in different aqueous and non-aqueous electrolytes were tested as a tool to assess the active surface area of Co films in relation to the current increase in voltammetric waves. The redox pairs' reaction was based on benzoquinone oxidation reduction, investigated in organic medium and onto Co films, whereas $[Ru(NH_3)_6]^{3+}$ was used on modified Co films by gold (AuCo) in aqueous solution. Importantly, for gold shielded Co metallic deposits, lead UPD was widely proved to be a surface structure process and sensitive to the active area of gold, herein used for indirect estimation of the sought increase of the area on the prepared Co deposits.[20,21]

2. Experimental

The DES was prepared using analytical-grade choline chloride (ChCl, Across Organics) and urea (Merck). ChCl and urea were dried in an oven at 70 °C for 24 h and placed in a desiccator, after which the DES was prepared by mixing amounts of ChCl and urea in a 1:2 molar ratio at approximately 50 ºC until becoming liquid. To prepare the cobalt bath, 0.1 M, 99% pure $CoCl_2{*}6H_2O$ salt (Merck) was dried at 100 ºC for 10 h until dehydrated and added to the DES. To dissolve the cobalt salt in the DES, the mixture was stirred and subsequently kept under vacuum and heating conditions for 24 h. This was made to reduce the water content until the optimal potential window on either gold and glassy carbon were obtained ensuring wide potential range to allow the deposition of metallic structures .[22–24]

To prepare the aqueous electrolytes for the analysis of the redox pairs and lead UPD the highest available pure lead perchlorate ($Pb(ClO_4)_2$), potassium perchlorate ($KClO_4$), were purchased from Sigma Aldrich-Merck company (99.99-99.999% purity degree) and hexaammineruthenium(III) chloride (>98%) from (Acros Organics) (99% purity) used to prepare fresh solutions for each experiment using Milli Q water. Organic electrolytes

were prepared using 1,4-benzoquinone (Sigma Aldrich, reagent grade), tetrabutylammonium hexafluorophosphate (Tokyo Chemical Industry (TCI) in acetonitrile for UHPLC, supergradient ACS (ApppiChemPanreac). All chemicals were used as received with the exception of 1,4-benzoquinone and tetrabutylammonium hexafluorophosphate. 1,4-benzoquinone was purified by flash column chromatography using CH_2Cl_2 as the eluent. Tetrabutylammonium hexafluorophosphate was recrystallized from absolute ethanol. Galvanic displacement was promoted using aqueous solutions of gold (III) chloride trihydrate >99.9% from Sigma-Aldrich.

Working electrodes used in this work were: a glassy carbon (GC) rod (0.0314 cm^2), a gold polycrystalline bead prepared by using Clavillier method,[25] and flat silicon pieces with a seed layer containing Ti(15nm) and Au(100nm), hereafter called "Si/Ti/Au". Specific pre-treatments were used for each of the surfaces. The glassy carbon electrode was polished to a mirror finish with alumina of different grades (3.75 and 1.87 µm; VWR Prolabo), cleaned ultrasonically for 2 min in water treated with the Milli Q system (Millipore), and dried with nitrogen prior to immersion in the solution. The pieces of Si/Ti/Au were cleaned with ethanol and acetone. The gold polycrystalline bead was cleaned by flame annealing followed by cooling down in air. Once cooled, all electrodes were immersed in the DES.

The Co electrodeposition in DES was performed in a thermostated cell with a three-electrode configuration at 70ºC. The reference electrode was Ag|AgCl mounted in a Lugging capillary containing the DES, whereas the counter electrode was a platinum spiral. The voltammetric analysis of the surface active area in either aqueous and organic electrolytes was carried in a three-electrode cell at room temperature. All potentials in this work were referred to the Ag|AgCl reference electrode.

Electrochemical measurements were carried out using a potentiostat (PGSTAT 12, Autolab). The morphology of the samples was analyzed using a field emission scanning electron microscope (FE-SEM; JSM-7100F Analytical Microscopy). Bragg–Brentano X-ray diffraction (BB-XRD, Brucker) with a Cu Kα radiation source (40 kV, 40 mA) was used to characterize the crystal structure of the samples. Diffractograms were recorded in the 2θ range between 25° and 90° with an offset of 1°. The chemical state of Co, O, and Au of the samples were evaluated via X-ray photoelectron spectroscopy (XPS, Physical Electronics 5500 Multi-technique System) at different depths from the surface down to approximately 300 nm. This was achieved by sputtering the deposits with Ar^+ ions (4 keV sputtering energy). Prior to characterization, the samples were exhaustively cleaned under warm water for the time needed to entirely remove the DES residues.

3. Results

3.1) Cobalt electrodeposition in DES.

Figure 1 shows the cyclic voltammetries (CVs) of the Co deposition on glassy carbon and in the DES. The CVs were conducted at three different cathodic potential limits. At the shortest selected cathodic potential limit (Fig. 1A a), red line) the CV displayed a voltammetric loop (pointed by red arrows in Fig. 1A) in the reduction or cathodic scan, indicating that the deposition follows a nucleation and growth mechanism. The counter peak in the anodic scan, centered around -0.3 V vs Ag|AgCl, corresponds to the oxidation of the deposited cobalt. Slightly increasing the cathodic potential limit (Fig. 1A b), black line) causes the CV to develop a diffusion peak at -1.25 V vs Ag|AgCl Interestingly, the counter oxidation peak became broader and less intense, a fact that was previously attributed to the surface passivation of the deposited Co by co-reduction together with the solvent [19,22,26]. The broadening and loosening of intensity in the oxidation peak becomes more accused by enlarging the cathodic potential limit (Fig. 1A c), dashed line)

towards the solvent reduction. As we claimed in our previous report, the reduction of the solvent, containing traces of water on the freshly deposited Co, increases the local pH and favors the formation of hydroxo- cobalt species, which passivates the surface.[19]

Figure 1B shows a group of chronoamperometric transients (j-t transients) recorded at different applied potentials between -1.04 V to -1.30 V vs Ag|AgCl. The j-t transients profiles evidences that the Co deposition follows a 3D nucleation and growth mechanism controlled diffused. First, the current increases until attaining a maximum, and then it decays exponentially by diffusion. Additionally, the j-t transients recorded at low overpotentials, show relatively good overlapping at long deposition times, confirming the linear diffusion control at this step. The profile of the j-transients is more defined at low applied potentials, probably because of the absence of solvent reduction interfering in the cobalt deposition at this potential range. Considerably increasing the applied potential affects the profile of the j-transient (Fig. 1B, c), green line). Curve c) in Fig. 1B reaches the current maximum at very low times due to instantaneous nucleation. Additionally, it does not overlap with the other curves at long times of deposition; instead, it displays higher current intensities. This is most likely caused by the overlapping of the solvent reduction currents with the Co deposition currents, suggesting that the optimal potential range for the deposition of metallic Co is below -1.20 V vs Ag|AgCl.

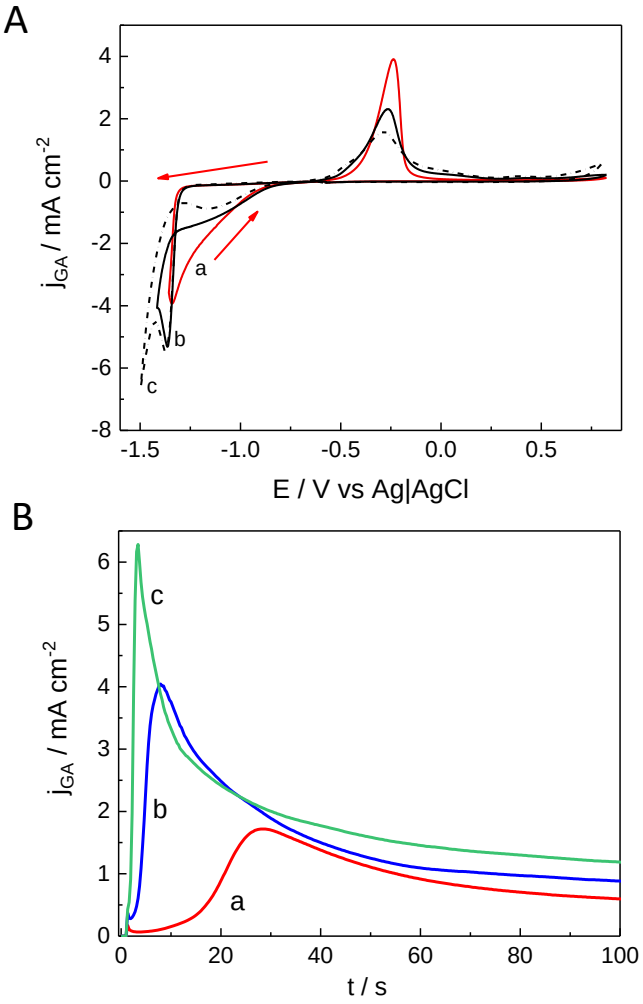

Figure 1: A) Cyclic voltammetries of the Co deposition in DES and on glassy carbon, at different cathodic potential limits: a) from 0.84 V to -1.35 V vs Ag|AgCl, b) from 0.84 V to -1.40 V Ag|AgCl and c) from 0.84 V to -1.50 V vs Ag|AgCl. Scan rate of 50 mV/s. B) Chronoamperometric transients of the Co deposition on glassy carbon and at different applied potential conditions: a) -1.04 V b) -1.22 V and c) -1.30 V vs Ag|AgCl.

Figure 2 shows the CVs of the Co deposition in DES but on the Si/Ti/Au substrate, at different cathodic potential limits, aiming to assess the applicability of the method to functionalize different substrates. Unlike the Co deposition on glassy carbon, the CV does not display any nucleation voltammetric loop at short applied potentials, i.e., when Co

deposition occurs on Au. This is due to a stronger bond between Co-Au rather than Co-Co, which activates the Co deposition at lower overpotentials compared with the thermodynamic reduction potential of bulk Co. Increasing the cathodic potential limit causes the current to rise until the diffusion peak is attained. Then, reversing the scan causes the appearance of a loop, indicating that, after the deposition of the first Co layers on the top of the substrate, Co nucleates and grows on Si/Ti/Au; this is similar to the reaction on glassy carbon. Enlarging the potential cathodic limit towards values, where the solvent reacts, causes the deposited Co film on Si/Ti/Au substrate to passivate, as evidenced in Figure 2B (curve d, yellow line).

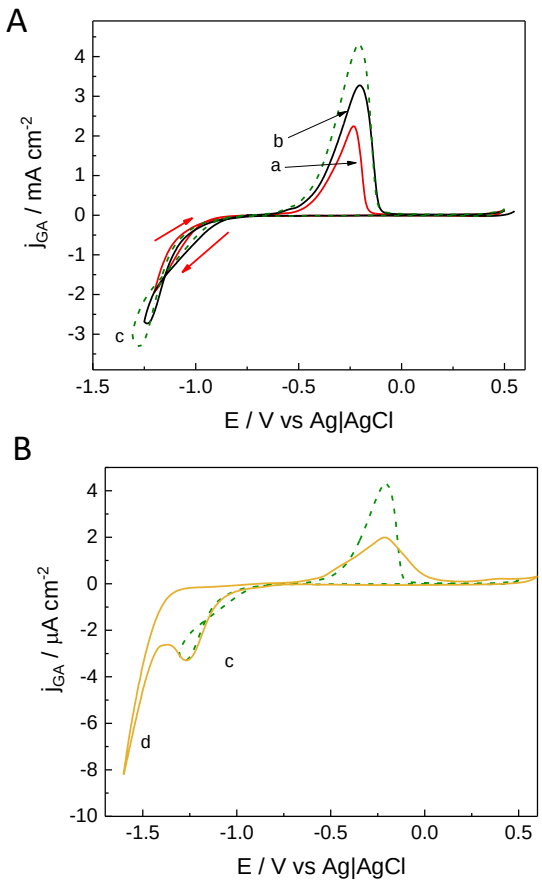

Figure 2: Cyclic voltammetries of the Co deposition in DES and on Si/Ti/Au substrate, at different cathodic potential limits: A) a) from 0.5 V to -1.20 V vs Ag|AgCl, b) from 0.84

V to -1.25 V vs Ag|AgCl and c) from 0.84 V to -1.30 V vs Ag|AgCl . B) c) from 0.84 V to -1.30 V vs Ag|AgCl and d) from 0.84 V to -1.6 V vs Ag|AgCl. Scan rate of 50 mV/s.

Figure 3 shows the SEM images of Co films deposited on Si/Ti/Au at two different overpotentials. Figure 3A shows the Co film at a low-moderate potential of -0.95 V. The Co film displays an interwoven morphology with ridge network of cobalt. This morphology is affected and distorted when the applied overpotential is increased to -1.25 V (Fig. 3B). This is due to the formation of hydroxo- and oxo species of Co, which modifies the original interwoven morphology.[19] Figures 3C and 3D show the respective XRD spectra of the films, which confirms the formation of multifaceted Co films. This also support that the amount of water in our pretreated DES is low enough or has little influence in shortening this potential window, allowing the deposition of metallic Co at moderate overpotentials[19]. The distribution of facets changes with the applied potential conditions for the Co deposition due to a change in the kinetics of the deposition process together with an increase on the formation of hydroxyl or oxygenated Co species. Notably, the intensity of the XRD peaks related to metallic Co is lower in the sample prepared at a higher overpotential (Figure 3D). This result also supports that higher overpotentials enhance the formation of an oxo hydroxo layer of Co that passivates the metallic surface, likely because of the reaction with water, which would tend to accumulate in the interface by highly polarizing the surface[27] or with the DES constituent that is a hydrogen donor. Similar results are obtained when the employed substrate was a glassy carbon electrode [19].

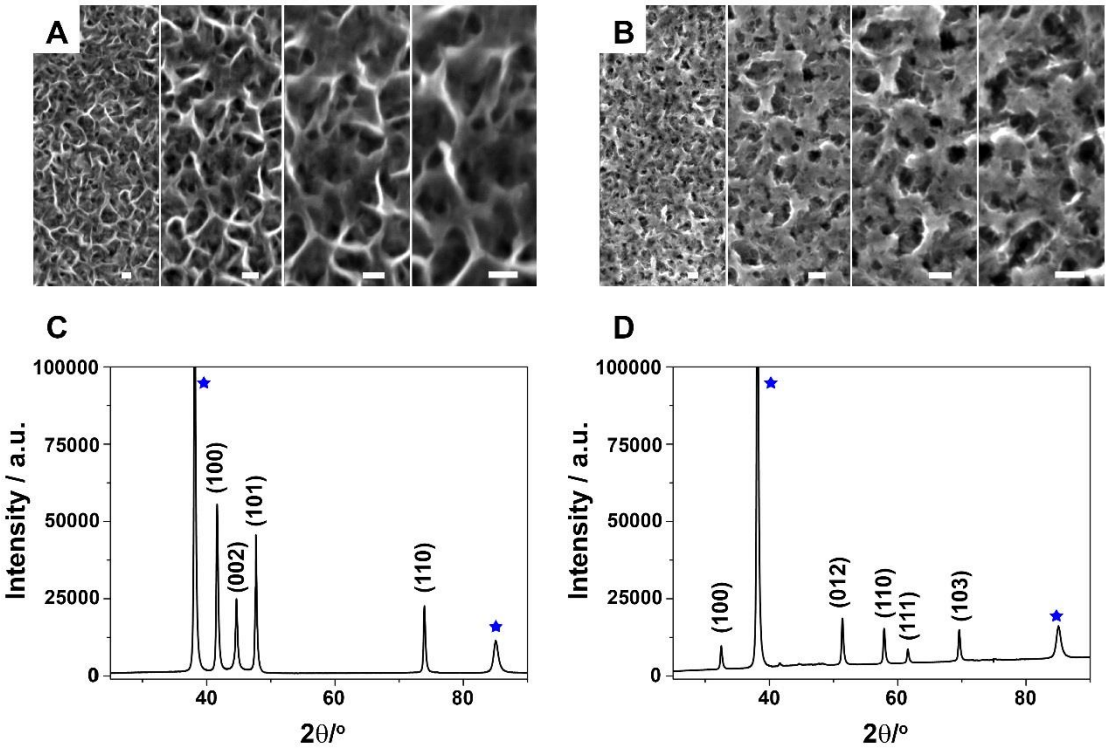

Figure 3: SEM images of the cobalt deposits prepared in DES on Si/Ti/Au at: A) -0.95 V and B) -1.25 V vs Ag|AgCl. Scale bar: 100 nm. C) and D) are the respective XRD spectra of each sample.

To corroborate the species formed at each selected potential range, XPS analysis of the two samples was also conducted. The XPS spectra were corrected by shifting all binding energies (BE) with respect to adventitious carbon (C 1s; C–C, C–H) at 284.8 eV. As shown in Figure 4A, the complex spectrum of Co 2p composed of two asymmetric peaks at approximately 778.2 and 793.1 eV corresponding to Co $2p_{3/2}$ and $2p_{1/2}$, respectively, confirmed that the deposits prepared at -0.95 V vs Ag|AgCl were mainly metallic cobalt. However, the presence of Co^{2+}, possibly $Co(OH)_2$, was also confirmed by the two plasmon-loss peaks resulting from the deconvolution of the asymmetric Co $2p_{3/2}$ peak [28–30]. The O 1s spectra of the deposits prepared at -1.25 V vs Ag|AgCl decomposed

into two components at BE approximately 530.1 and 531.8 eV, which coincided with the assignment of metal oxide bonds and the adsorption of OH groups on the surface of the Co deposit [31,32]. All these data confirmed that Co(0) was the predominant species in the deposits prepared at -0.95 V vs Ag|AgCl. By contrast, the important satellite peaks at approximately 783.1 and 801.3 eV corresponding to Co $2p_{3/2}$ and $2p_{1/2}$, respectively, ascribed to Co(II), confirmed that, at more negative potentials, richer oxy-hydroxy cobalt deposits were obtained (Figure 4B). Consistently, the O 1s spectra of deposits prepared at -1.25 V vs Ag|AgCl, decomposed intro three components, which coincided with the assignment for CoO, $Co(OH)_2$ and structural water, confirmed the presence of oxy-hydroxy cobalt [19,29,31]. No Au species were detected in these XPS analyses.

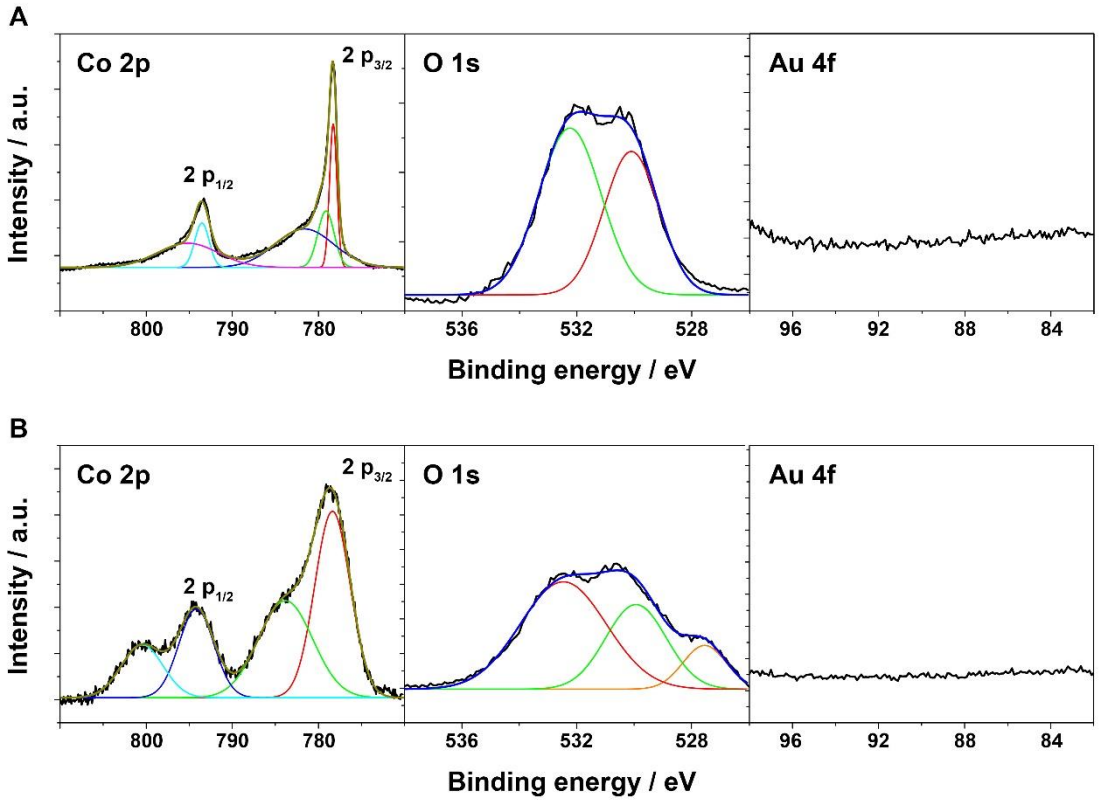

Figure 4: XPS analysis of the Co deposits on Si/Ti/Au and at different applied potential conditions: A) -0.95 V vs Ag|AgCl and B) 1.25 V vs Ag|AgCl.

The *in situ* electrochemical study of the Co deposition in DES, combined with the morphological and chemical ex situ analysis of the prepared films, provide the evidence that the amount of oxo and hydroxo cobalt species can be tuned by increasing the applied overpotentials conditions. These oxygenated cobalt species considerably affect the morphology and crystallinity of the prepared samples. The formation of oxygenates is minimized, or even suppressed, by applying moderate and low overpotentials, and Co metallic structures are obtained instead. The decoration of these substrates with cobalt shows that in the DES solvent, the growth is modulated by the solvent characteristics and the electrodeposition conditions.

3.2) Voltammetric evaluation of effective surface modification after cobalt deposition

As the final interest of these materials is the preparation of surface-carriers and catalysts with high surface/volume ratio, we test the use of the voltammetric technique as a tool to characterize the effective area of Co films prepared at different electrodeposition conditions. At first, we decide to test organic species for which reversible processes have previously been described at considerable negative potential ranges. Benzoquinone was selected as a redox probe to test the active area of Co films [33,34]. After depositing Co on the substrate, the deposits were consecutively cleaned with small portions of warm water. A three electrode cell, containing 4 mM 1,4-benzoquinone in acetonitrile, was used with 0.1 M tetrabutylammonium hexafluorophosphate as supporting electrolyte. Figure 5A shows the reaction of 1,4 benzoquinone in the pristine Si/Ti/Au substrate. The 1,4-benzoquinone molecule's complete conversion to 1,4-hydroquinone shows two reversible redox pair of peaks involving two electron transfer steps. These two steps correspond to the successive outer sphere exchange of two electrons between the probe and the surface, according to the mechanism for the reduction of two consecutive α,β-unsaturated

carbonyls. The process was demonstrated to be very sensitive to the oxygen presence; thereby, the solution was carefully deoxygenated with argon [33,34].

The voltammetric experiments were performed both on Si/Ti/Au substrate and cobalt deposits in order to assess the suitability of the process on these substrates. Expected behavior was observed, and two clear pairs of reversible peaks were recorded which peak potentials were little dependent of the substrate nature. As the potential value of the first electron exchange is sufficiently negative to avoid the cobalt oxidation, experiments using the Co deposits were performed by scanning the potential range of the first voltammetric couple of peaks (between -0.35 V to -0.70 V vs Ag|AgCl). We observed that it is convenient to limit the potential window up to -0.70 V vs Ag|AgCl in the cathodic scan, to avoid the overlapping of the current related to the second electron transfer process which, in addition, is more sensitive to the presence of oxygen.

Various Co deposits were prepared at different applied potentials, fixing the same circulated charge to better compare the possible effect of the applied potential over the increase of the effective area versus the geometrical one. The selected preparation potential range was wide and resulted in the realization of different metallic and oxo hydroxo cobalt species. Figure 5B shows the cyclic voltammograms recorded in the 4 mM benzoquinone solution, on pristine Si/Ti/Au substrates (curve a), dashed line), and on the covered substrate by Co (curves b), c) and d)). At first, it was confirmed that the peak potential position is slightly sensitive to the electrode nature and l appears at similar values for cobalt and for gold substrates, showing good reproducibility.

Comparing the recorded curves on the prepared Co deposits, with the CV of the Si/Ti/Au substrate, we observed an increase in intensity of the current peak as the overpotential applied for the Co deposition increases (Fig. 5B). Interestingly, once a threshold overpotential value was reached, the associated current peak began to diminish (Fig. 5C).

The current increase is not linear with the applied potential, and it becomes less notorious increasing the applied overpotential. On the other hand, the current decay occurs at the potential values at which the influence of the hydroxylated species formation is more prevalent. These results show that at the potential range at which metallic cobalt deposits, the associated current probe increases and corresponds to the observed ridge morphology. In contrast, at the conditions at which FE-SEM evidences a smooth morphology generated by the increase of the amount of hydroxylated species codeposition, the probe current diminishes. The decrease of the peak current intensity could be caused by the low conductivity and low electrochemical activity of the oxo hydroxo species of cobalt, which reduces the number of effective active sites for the benzoquinone to react.

Although this method involves an external sphere probe, for this kind of cobalt deposits in which open morphology is observed, it seems a good tool to qualitatively estimate the effective surface modification as a function of the applied electrodeposition conditions. The *in situ* voltammetric characterization, allows to discriminate the potential range at which metallic cobalt samples, with ridge morphology induced by the DES, are obtained. However, the use of both organic medium and organic species, together with the high sensitivity of benzoquinone, which requires a strict experimental procedure, encouraged us to test an alternative probe in an aqueous medium.

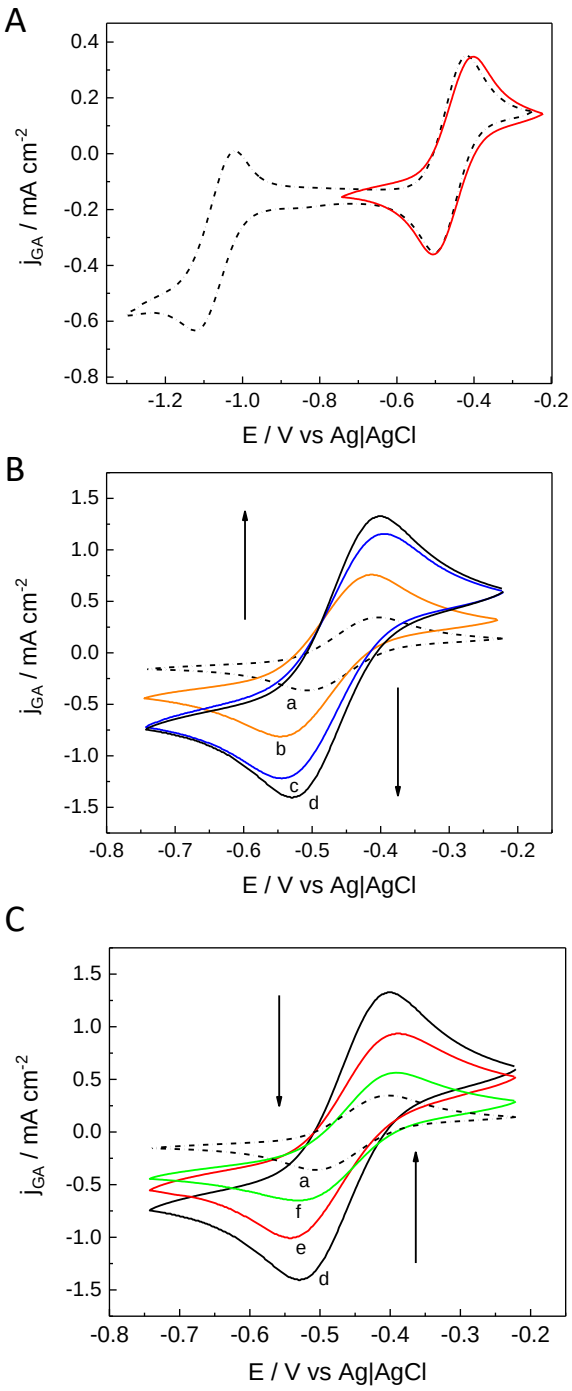

Figure 5: A) Cyclic voltammetries of the 1,4-benzoquinone 4 mM solution in acetonitrile plus 0.1 M tetrabutylammonium hexafluorophosphate on: A) Si/Ti/Au , B) a) Si/Ti/Au and on Co films deposited at different applied potentials : b) -0.90 V, c) -1.03 V and d) -1.10 V vs Ag|AgCl and C) d) 1.10 V, e) -1.20 V and f) -1.32 V vs Ag|AgCl . Scan rate

of 50 mV/s. The arrows in B) and C) indicate the increase or decrease of the current peak, respectively, as the applied potential increases.

The selected alternative aqueous probe was a solution containing 0.02 M of $Cl_3[Ru(NH_3)_6]$ in KCl 0.2 M. The associated redox process, showing good reversibility, is the eq. (1) [35,36]:

$$[Ru(NH_3)_6]^{3+} + e^- \underset{\leftarrow}{\overset{\rightarrow}{}} [Ru(NH_3)_6]^{2+} \qquad (1)$$

On the Si/Ti/Au, the electrochemical window at which this specific outer sphere electron transfer takes place, moves to more positive values, being established between -0.35 and 0.05 V (Fig. 6A curve a). Consequently, the voltammetric feature of the $[Ru(NH_3)_6]^{3+}$ reacting on the deposited Co films, overlapped with an additional current corresponding to incipient cobalt oxidation (Fig. 6A curve b), thereby limiting the analysis of the active area with this redox probe. In order to prevent the Co oxidation, the prepared Co films were shielded by gold. The gold coverage was performed via spontaneous galvanic displacement reaction. In order to assure that the Co surface is completely covered by gold, the immersion time of cobalt deposits was established to be 60 seconds using a 1mM tetrachloroaurate (III) solution ($[AuCl_4]^-$). Gold (III) was reduced on top of the surface oxidizing the cobalt atoms to Co(II) state, being dissolved into the solution. Interestingly, the CVs of the $[Ru(NH_3)_6]^{3+}$on Co films and Co films covered by gold (AuCo films) displayed similar current intensities, despite that the curve recorded on Co slightly overlapped with the onset of the Co oxidation. This similarity in current density supports that gold on top of Co has a little effect on the active area of Co.

Figures 6B and 6C show the cyclic voltammetries recorded on AuCo films, prepared at different applied potential conditions and after the treatment with the Au(III) solution. The recorded CVs in Figures 6B and 6C display an increase of the current density until a

threshold potential is attained, similar to what occurred with the benzoquinone probe in organic media. This threshold potential was around -1.1 V vs Ag|AgCl (Figure 6B curve d). Higher applied potential conditions for the preparation of Co films causes a continuous decrease of the recorded current peak of the redox probe (Fig. 6C), due to modification of the surface by formation of oxo- and hydroxospecies of Co. The threshold potential value was similar than that observed in benzoquinone solution, as expected, confirming that the method qualitatively informs about the superficial change of the deposit.

Experiments performed on deposits prepared at fixed potentials at which metallic cobalt is deposited showed that, once a certain charge value is attained, the recorded peak current slightly changes, as depicted in Figure 6D. This could be interpreted as that, once the overall coverage of the substrate is reached, the effective area remains stationary, demonstrating that this medium enhances the increase of effective surface.

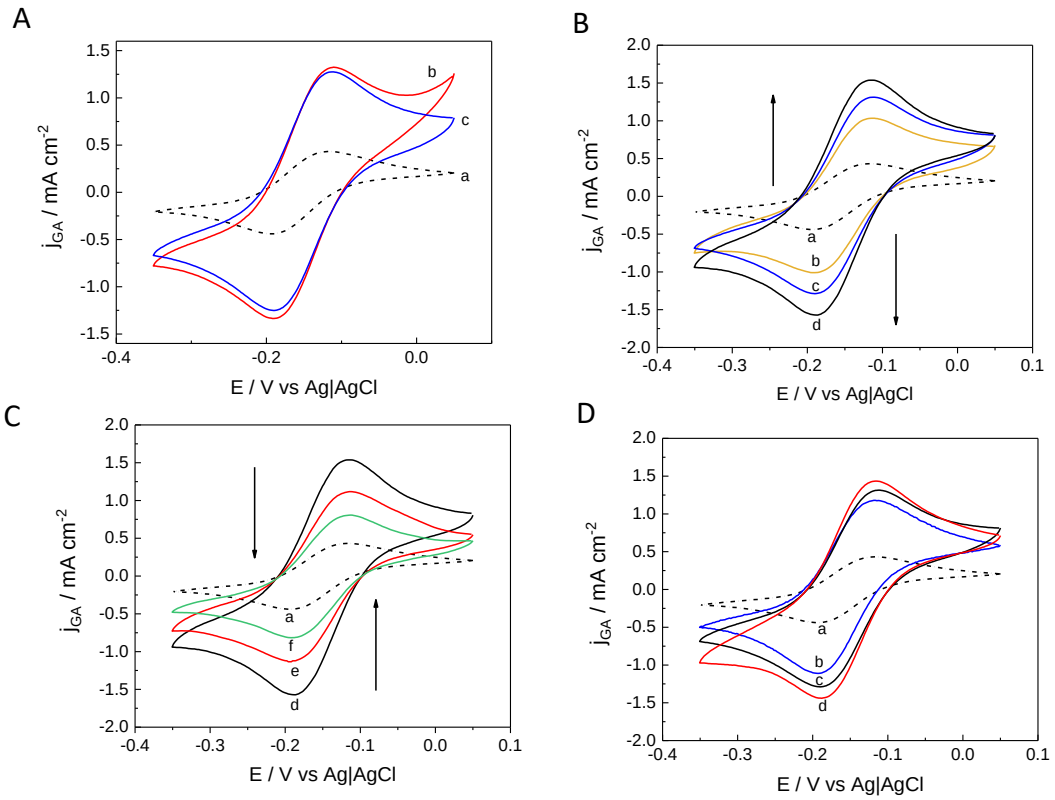

Figure 6: Cyclic voltammetries of the hexaammineruthenium (III) chloride reaction in 2 mM aqueous solution on: A) a) pristine Si/Ti/Au, b) Co film deposited at -1.03 V and on c) Co film deposited at -1.03 V vs Ag|AgCl modified by Au via galvanic displacement reaction and during 60 s in a 1 mM $[AuCl_4]^-$ solution. AuCo films deposited at different applied potentials. B) a) pristine Si/Ti/Au, b) -0.90 V, c) -1.03 V and d) -1.10 V vs Ag|AgCl and C) d) -1.10 V, e) -1.20 V and f) -1.32 V vs Ag|AgCl. D) Cyclic voltammetries of the hexaammineruthenium(III) chloride reaction on Co films deposited at -1.03 V vs Ag|AgCl and modified by gold via galvanic displacement, at different circulated charges a) pristine Si/Ti/Au, b) -75 mC, c) -100 mC and d) -150 mC. Scan rate of 50 mV/s. The arrows in B) and C) indicate the increase or decrease of the current peak, respectively, as the applied potential increases.

Furthermore, in order to assess the impact of the galvanic displacement reaction between gold and cobalt on the original morphology of the Co deposits in Figure 3, the cobalt

samples were also imaged by SEM after being treated with the 1 mM $[AuCl_4]^-$ solution. Figures 7A and B show that the Co film covered by Au, keep the main interwoven skeleton of the original Co film (see magnification in Fig. 7A), although it has been slightly affected by the presence of Au. Au shielding on Co has generated more rounded and smother edges. Interestingly, the XRD spectra of the corresponding Au-modified Co films essentially display the same group of crystallographic Co facets as the original Co samples in Figures 3C and 3D (Fig. 7C and D). The main difference is that the intensity of the Co peaks has decreased, probably because of the covering of Co by Au, although Au on top of Co causes little changes in the crystallinity of the Co film.

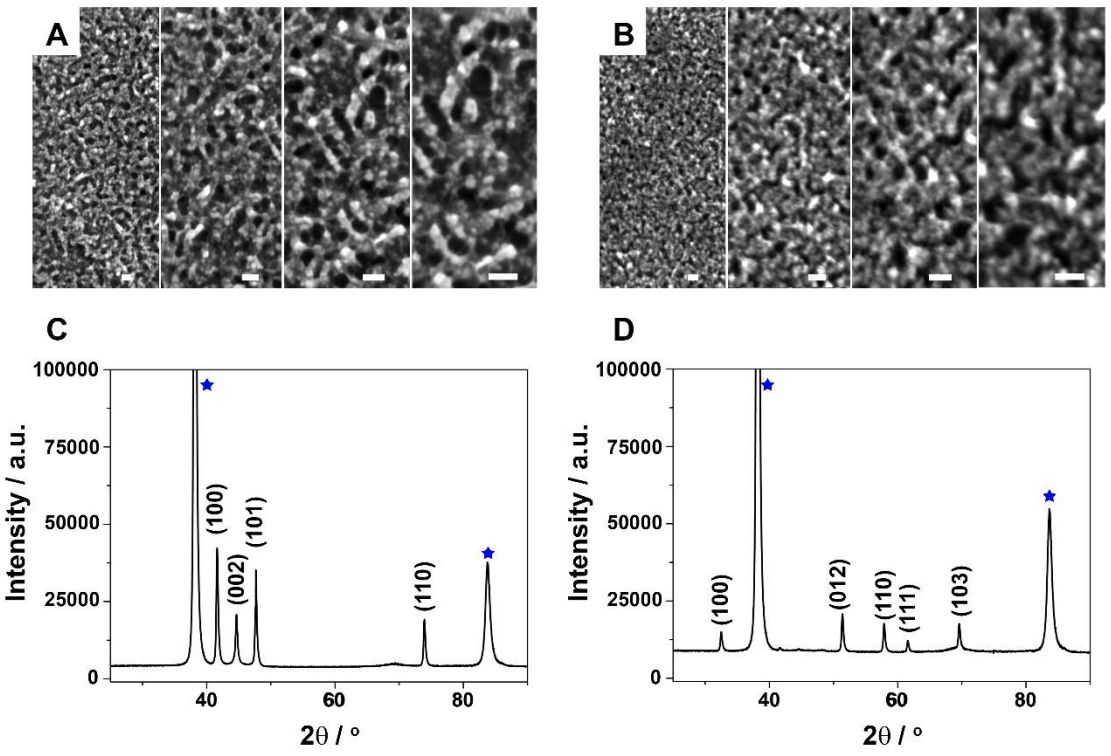

Figure 7: SEM images of the cobalt deposits after modification by galvanic displacement of Au prepared on Si/Ti/Au substrate at A) 0.95 V and B) -1.25 V vs Ag AgCl. Scale bar: 100 nm. C) and D) are the respective XRD spectra.

The XPS analysis (Fig. 8) of the samples after the galvanic displacement confirmed that Au was effectively deposited as no Co signals were visible during various Ar^+ sputter cycles (< 200 nm). Conversely, as shown in Figure 8, the Au 4f spectra of deposits exhibited two asymmetric peaks at 84.8 and 88.2 eV corresponding to $4f_{7/2}$ and Au $4f_{5/2}$, respectively, suggesting the coexistence of Au(0) and Au(I) [37,38]. However, the weakness of Au(I) signals also indicates that the majority of the Au existed in the form of Au(0).

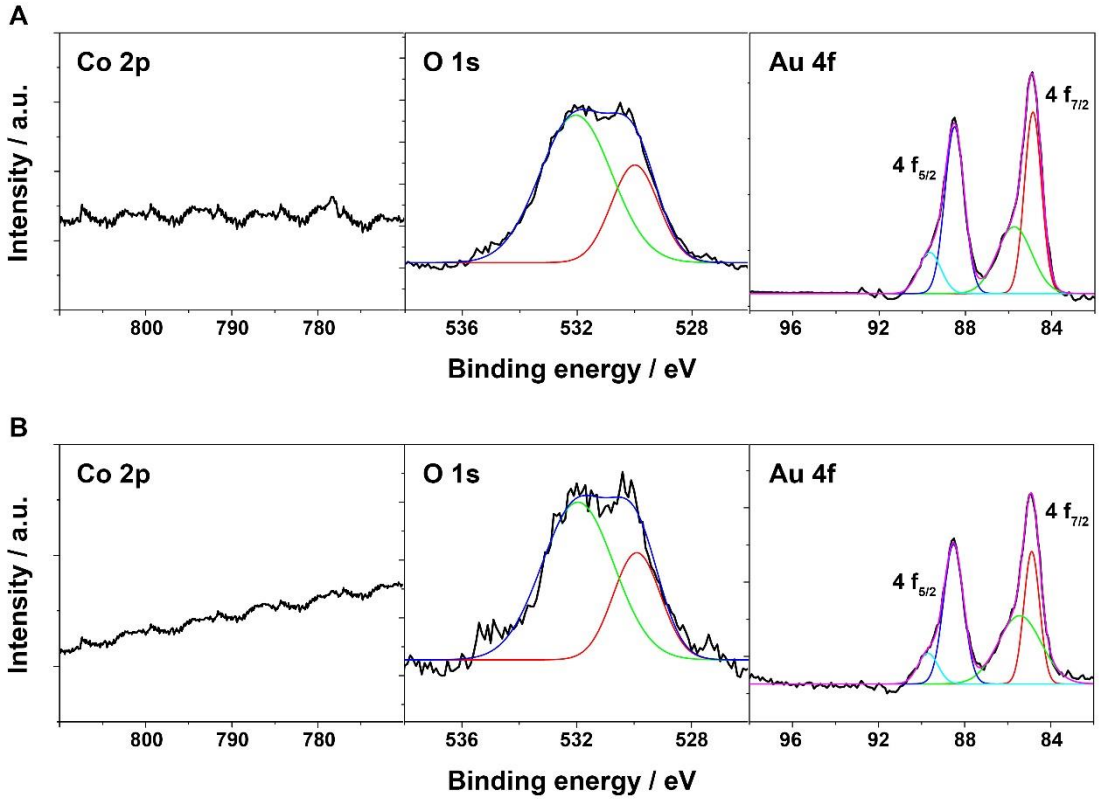

Figure 8: XPS analysis of the Au deposited galvanostatically on the Co films on Si/Ti/Au substrate and at different conditions: A) -0.95 V vs Ag|AgCl and B) -1.25 V vs Ag|AgCl.

In summary, both voltammetric results, in combination with XPS analysis, demonstrated that this method is a useful and agile strategy for the evaluation of the characteristics of

prepared cobalt deposits. The results also showed that the gold-shielding strategy does not disturb the evaluation method.

3.3) Galvanic displacement of Co by Au, and lead UPD on the Au layer

As an alternative and quantitative method, metal UPD on freshly deposited metallic Co samples, was conducted to evaluate the number of new active sites created on the Co film in DES. Metal UPD is a surface process highly sensitive to the number of active sites and structure of the employed electrode. In particular, lead UPD has been widely described on different gold single crystal surfaces,[20,21] but it has been also extensively used for surface characterization and determination of domains and sites in a variety of polycrystalline and shaped gold nanoparticles.[39–41] Herein, indirect lead (Pb) UPD on Co films prepared at low-moderate overpotentials and superficially modified by gold, was assessed. As Pb UPD does not take place on a Co surface, because Co oxidizes in the potential region at which Pb UPD occurs, the first layers of Co were also galvanically displaced by Au, as described in the previous section. Then, the Pb UPD on the nanostructured Au-Co film was performed to indirectly estimate the active area of the Co films.[42] Before the galvanic displacement, Co was electrodeposited both on an Au polycrystalline bead, with no roughness index, and on a Si/Ti/Au, to assess the effect of using substrates of different geometry and structure on the active area of deposited Co films. The selected applied potential to prepare the Co films was around -1.0 V vs Ag|AgCl to avoid the formation of oxygenated or hydroxyl Co species which block the surface.

Pb UPD on a polycrystalline Au bead was firstly conducted (Fig. 9A). A Au bead electrode was prepared by thermal annealing of a Au wire. This implies that the polycrystalline Au bead has the facet distribution which is thermodynamically more favorable. The CV of Pb UPD on the Au bead in Fig. 9A, shows the typical group of

voltammetric features reported in literature, and evolves an integrated charge of around 300 mC cm^{-2}.[20,21,43] Figure 9B shows the Pb UPD CV on a Si/Ti/Au, which displays a profile completely different to that obtained on an Au bead. This suggests that the Si/Ti/Au has a different orientation, and some facets may predominate over others. This different orientation is likely induced by the Si support.

Repeating the same protocol described above, the galvanic displacement between Au and Co was carried out by immersing the Co deposits in a 1 mM [$AuCl_4$] solution for 1 minute. Then, the Pb UPD was conducted on the Au-Co film deposited on either a gold bead (Fig. 9C) or a Si/Ti/Au substrate (Fig. 9D). Both Figure 9C and Figure 9D display the CVs of the Pb UPD on the AuCo film on each substrate (solid red line), and on the pristine Au substrate (dashed black line), for comparison. A substantial increase of the current intensity of three to four times is observed on the Au layer deposited on the Co film by galvanic displacement. Interestingly, the Pb UPD voltammetric profile on the AuCo film is the same as the Pb UPD on an Au bead, even when the employed substrate was a Si/Ti/Au (Fig. 9B and D). A plausible explanation to this result is that the specific orientation of the Au substrate has no effect on the growth of the Co deposit, at sufficiently high circulated charges, i.e., by increasing the thickness of the Co deposit. In experiments from Figures 9C and 9D (red lines), the Co film deposition was performed at moderated overpotential (-1.0 V vs Ag|AgCl) after circulating a charge above 100 mC cm^{-2}, aiming to obtain both thick and metallic Co films.

In Table 1, the integrated charge values of the Pb UPD and roughness factor of prepared AuCo films by galvanic displacement are summarized. To calculate the charge from the CVs, the voltammetric curves obtained in the cathodic scan were integrated (Table 1). Interestingly, an increment of the electroactive area of 3.3 and 4.5 were obtained when the AuCo film was deposited on an Au bead and on a Si/Ti/Au substrate, respectively.

Importantly, the estimation of the active area by integration of the voltammetric charge assumes one electron transfer per atom of surface metal with a lead coverage of approximately 0.5 on Au. The calculated charge values included in Table 1 are proportional to the active area of the Au layer deposited on Co by galvanic displacement. The active area of the pristine Co deposit can slightly vary, depending on the stoichiometric coefficients of Co and Au in the galvanic displacement reaction. The most likely elementary reaction occurring during the galvanic displacement is:

$$3\text{Co-Substrate} + 2Au^{3+} \rightarrow 3Co^{2+} + 2\text{Au-Substrate} \quad (2)$$

This would imply that 3 atoms of Co are replaced by every 2 atoms of Au in the galvanic reaction. This means that the real active area of Co is most likely underestimated with this method of Pb UPD on the Au layer covering the Co films. Assuming that 3 atoms of Co are replaced by every 2 atoms of gold, the abovementioned roughness factors for Co would be corrected from 3.3 to 4.95 and from 4.5 to 6.75. These results suggest that the effective area of deposited Co in DES may range between 4 to 6 times higher than the geometric area of the employed substrate. The order of magnitude is in line with the results obtained in the previous section, which showed an increase in intensity of the benzoquinone voltammetric feature of 4 to 5 times higher than the peak in the pristine substrate, depending on the applied potentials.

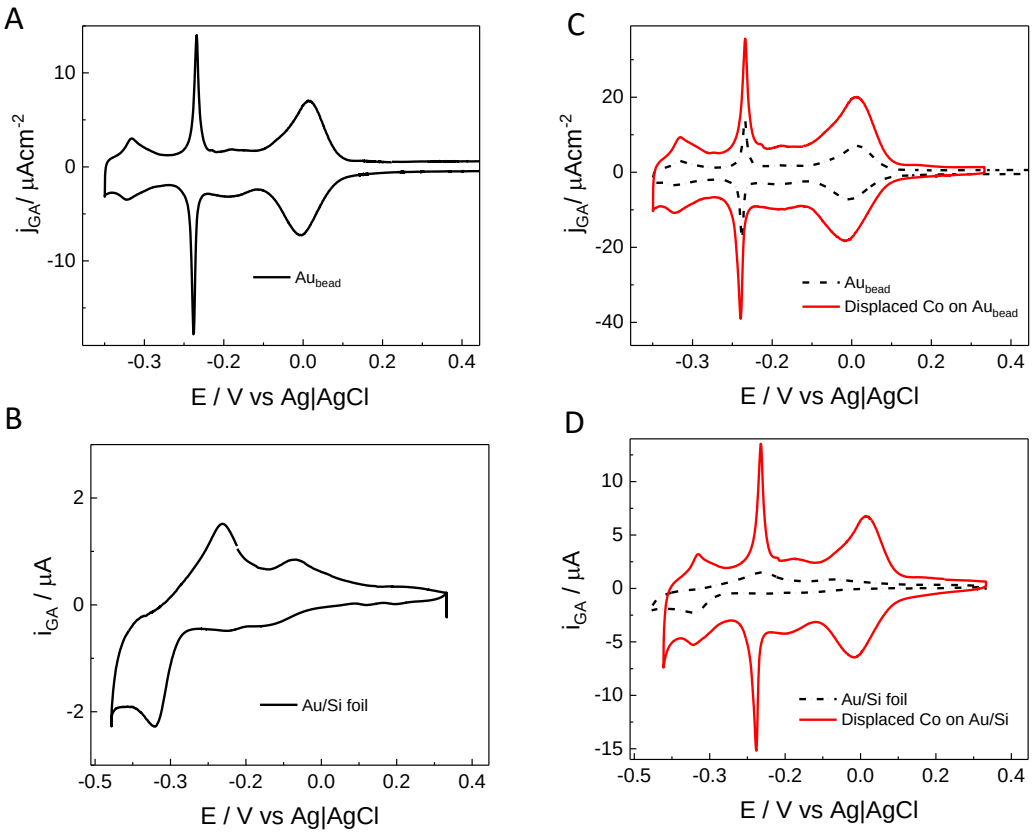

Figure 9: Cyclic voltammetries of the Pb UPD, from a 2 mM Pb^{2+} plus 0.1 M $KClO_3$, pH=3 on different surfaces: A) Gold polycrystalline bead, B) Si/Ti/Au. Pb UPD on a Au nanostructured layer prepared by galvanic displacement between Au and the Co film electrodeposited at a moderate overpotential of -1.0 V vs Ag|AgCl on C) Au polycrystalline bead, at -30 mC, D) Si/Ti/Au, at -40 mC. The galvanic displacement is carried out during 60 seconds. Scan rate of 5 mV/s.

Table 1: Charge integrated from the voltammetric cathodic region of the lead UPD on different Au substrates and Au covering Co after performing the galvanic displacement reaction, from Figure 9.

	Charge / μC	Roughness factor	roughened Co $3Co_{atoms}/2Au_{atoms}$
Au poly bead	45.4	1	
Roughened Au	156.8	3.3	4.95
Si/Ti/Au	108	--	
Roughened Si/Ti/Au	488	4.5	6.75

Despite the slight change in morphology induced by Au, with little effect on the crystallinity of the film, and the uncertainness in the number of Co atoms replaced by Au in the galvanic displacement reaction, the obtained results provide the evidence that high extended surfaces areas of Co are obtained in DES. These results also show alternative ways for the nanostructuring of highly active metal-surfaces, such as Au, for catalyst design.

Conclusions

Herein we have investigated the effect of the applied potential conditions in the effective surface area of Co films electrodeposited in choline chloride plus urea deep eutectic solvent. Several *in situ* voltammetric methods in combination with *ex situ* characterization techniques were tested to assess the changes in the effective active area. We observed that the applied potential conditions affect the ratio between metallic Co and oxidized Co species. Increasing the applied potential induces the appearance of oxo hydroxo species which passivates the surface. These species affect the interwoven morphology of metallic

Co induced by the DES. Instead, the surface passivation induces smoothening of the edges of the nanostructured Co films.

Benzoquinone reaction in organic media and hexaammineruthenium(III) reaction in aqueous media were used as an evaluation tool for *in situ* analysis of the increase in the active surface area of Co films deposited at different applied potential conditions. These two reactions involucre outer sphere electron transfer reactions. An increase of the current intensity of these two reactions was observed as the applied potential conditions were raised up to a threshold potential. At potentials above this threshold, the current intensity starts to decrease. This behavior was addressed to the formation of oxo hydroxo Co species, which decrease the number of active site position in the deposited film, results in line with the *ex situ* characterization of the deposits. Although the out sphere probes normally are sensitive to geometrical area, for this interwoven morphology the results indicate that could detect roughly noticeable changes in effective surface. The use of these two outer sphere redox pair was demonstrated to be a useful tool to qualitatively assess the modification in the effective area and determine the potential region at which metallic Co is optimally obtained.

Lead UPD on Co films covered by a gold layer, generated via galvanic displacement reaction, was also evaluated as a quantitative tool to test the increase in the effective surface area. It was observed that the Co films modified by gold presented an active surface area 4 to 6 times larger than the pristine area of the Si/Ti/Au substrates. The *ex situ* characterization of the Co modified films by gold showed that the covering of Co by Au causes a slight change in the morphology of the deposits, inducing rounded edges, although the interwoven original skeleton was maintained. The XRD analysis revealed that gold causes little impact in the crystallinity of the original Co film. Additionally, the reaction of hexaammineruthenium(III) on the Co film covered by gold was similar in

intensity as in the non-covered Co film deposited under the same conditions, suggesting that the layer of Au slightly influences the effective surface area of the nanostructured Co film. These results suggest that Pb UPD can be also employed for indirect and qualitative examination of the effective surface area of the Co films prepared by electrodeposition technique in DES.

AUTHOR INFORMATION

*Corresponding author:

E-mail: paula.sebastián25@gmail.com

ORCID

Paula Sebastián-Pascual: 0000-0001-7985-0750

Elvira Gómez Valentín: 0000-0002-9223-6357

Albert Serrà Ramos: 0000-0003-0147-3400

Notes

The authors declare no competing financial interest.

ACKNOWLEDGMENT

Acknowledgements

This work was supported by the TEC2017-85059-C3-2-R projects (financed by the *Fondo Europeo de Desarrollo Regional*, FEDER) from the Spanish *Ministerio de Economía y Competitividad* (MINECO). The authors also thank the CCiT-UB for the use of their equipment.

REFERENCES:

[1] A. Serrà, J. García-Torres, Electrochemistry: A basic and powerful tool for

micro- and nanomotor fabrication and characterization, Appl. Mater. Today. 22 (2021). https://doi.org/10.1016/j.apmt.2021.100939.

[2] Y. Shao, J. Wang, H. Wu, J. Liu, I.A. Aksay, Y. Lin, Graphene based electrochemical sensors and biosensors: A review, Electroanalysis. 22 (2010) 1027–1036. https://doi.org/10.1002/elan.200900571.

[3] D. Chen, H. Feng, J. Li, Graphene oxide: Preparation, functionalization, and electrochemical applications, Chem. Rev. 112 (2012) 6027–6053. https://doi.org/10.1021/cr300115g.

[4] D.R. Dekel, Review of cell performance in anion exchange membrane fuel cells, J. Power Sources. 375 (2018) 158–169. https://doi.org/10.1016/j.jpowsour.2017.07.117.

[5] T. Le Manh, E.M. Arce-Estrada, M. Romero-Romo, I. Mejía-Caballero, J. Aldana-González, M. Palomar-Pardavé, On Wetting Angles and Nucleation Energies during the Electrochemical Nucleation of Cobalt onto Glassy Carbon from a Deep Eutectic Solvent, J. Electrochem. Soc. 164 (2017) D694–D699. https://doi.org/10.1149/2.1061712jes.

[6] T. Le Manh, E.M. Arce-Estrada, I. Mejía-Caballero, J. Aldana-González, M. Romero-Romo, M. Palomar-Pardavé, Electrochemical Synthesis of Cobalt with Different Crystal Structures from a Deep Eutectic Solvent, J. Electrochem. Soc. 165 (2018) D285–D290. https://doi.org/10.1149/2.0941807jes.

[7] P. Cojocaru, L. Magagnin, E. Gomez, E. Vallés, Using Deep Eutectic Solvents to electrodeposit CoSm films and nanowires, Mater. Lett. 65 (2011) 3597–3600. https://doi.org/10.1016/j.matlet.2011.08.003.

[8] P. Sebastián, E. Torralba, E. Vallés, A. Molina, E. Gómez, Advances in Copper Electrodeposition in Chloride Excess. A Theoretical and Experimental Approach, Electrochim. Acta. 164 (2015) 187–195. https://doi.org/10.1016/j.electacta.2015.02.206.

[9] M. Li, Z. Wang, R.G. Reddy, Cobalt electrodeposition using urea and choline chloride, Electrochim. Acta. 123 (2014) 325–331. https://doi.org/10.1016/j.electacta.2014.01.052.

[10] P. Guillamat, M. Cortés, E. Vallés, E. Gómez, Electrodeposited CoPt films from a deep eutectic solvent, Surf. Coatings Technol. 206 (2012) 4439–4448. https://doi.org/10.1016/j.surfcoat.2012.04.093.

[11] A. Serrà, N. Gimeno, E. Gómez, M. Mora, M.L. Sagristá, E. Vallés, Magnetic Mesoporous Nanocarriers for Drug Delivery with Improved Therapeutic Efficacy, Adv. Funct. Mater. (2016). https://doi.org/10.1002/adfm.201601473.

[12] L.I.N. Tomé, V. Baião, W. da Silva, C.M.A. Brett, Deep eutectic solvents for the production and application of new materials, Appl. Mater. Today. 10 (2018) 30–50. https://doi.org/10.1016/j.apmt.2017.11.005.

[13] O.S. Hammond, D.T. Bowron, K.J. Edler, Liquid structure of the choline chloride-urea deep eutectic solvent (reline) from neutron diffraction and atomistic modelling, Green Chem. 18 (2016) 2736–2744. https://doi.org/10.1039/c5gc02914g.

[14] M. Palomar-Pardavé, J. Aldana-González, L.E. Botello, E.M. Arce-Estrada, M.T. Ramírez-Silva, J. Mostany, M. Romero-Romo, Influence of Temperature on the Thermodynamics and Kinetics of Cobalt Electrochemical Nucleation and Growth, Electrochim. Acta. 241 (2017) 162–169.

https://doi.org/10.1016/j.electacta.2017.04.126.

[15] E. Gómez, E. Vallés, Thick cobalt coatings obtained by electrodeposition, J. Appl. Electrochem. 32 (2002) 693–700. https://doi.org/10.1023/A:1020194532136.

[16] E. Gómez, M. Marín, F. Sanz, E. Vallés, Nano- and micrometric approaches to cobalt electrodeposition on carbon substrates, J. Electroanal. Chem. 422 (1997) 139–147. https://doi.org/10.1016/S0022-0728(96)04899-1.

[17] J. García-Torres, E. Gómez, E. Vallés, Modulation of magnetic and structural properties of cobalt thin films by means of electrodeposition, J. Appl. Electrochem. 39 (2009) 233–240. https://doi.org/10.1007/s10800-008-9661-9.

[18] A. Cojocaru, M.L. Mares, P. Prioteasa, L. Anicai, T. Visan, Study of electrode processes and deposition of cobalt thin films from ionic liquid analogues based on choline chloride, J. Solid State Electrochem. 19 (2015) 1001–1014. https://doi.org/10.1007/s10008-014-2711-9.

[19] M. Landa-Castro, P. Sebastián, M.I. Giannotti, A. Serrà, E. Gómez, Electrodeposition of nanostructured cobalt films from a deep eutectic solvent: Influence of the substrate and deposition potential range, Electrochim. Acta. (2020) 136928. https://doi.org/https://doi.org/10.1016/j.electacta.2020.136928.

[20] A. Hamelin, J. Lipkowski, Underpotential deposition of lead on gold single crystal faces: Part II. General discussion, J. Electroanal. Chem. Interfacial Electrochem. 171 (1984) 317–330. https://doi.org/https://doi.org/10.1016/0022-0728(84)80123-0.

[21] A. Hamelin, Underpotential deposition of lead on single crystal faces of gold:

Part I. The influence of crystallographic orientation of the substrate, J. Electroanal. Chem. Interfacial Electrochem. 165 (1984) 167–180. https://doi.org/https://doi.org/10.1016/S0022-0728(84)80095-9.

[22] E.A. Mernissi Cherigui, K. Sentosun, P. Bouckenooge, H. Vanrompay, S. Bals, H. Terryn, J. Ustarroz, Comprehensive Study of the Electrodeposition of Nickel Nanostructures from Deep Eutectic Solvents: Self-Limiting Growth by Electrolysis of Residual Water, J. Phys. Chem. C. 121 (2017) 9337–9347. https://doi.org/10.1021/acs.jpcc.7b01104.

[23] P. Sebastián, M.I. Giannotti, E. Gómez, J.M. Feliu, Surface Sensitive Nickel Electrodeposition in Deep Eutectic Solvent, ACS Appl. Energy Mater. 1 (2018) 1016–1028. https://doi.org/10.1021/acsaem.7b00177.

[24] C. Du, B. Zhao, X.-B. Chen, N. Birbilis, H. Yang, Effect of water presence on choline chloride-2urea ionic liquid and coating platings from the hydrated ionic liquid, Sci. Rep. 6 (2016) 29225. https://doi.org/10.1038/srep29225.

[25] J. Clavilier, R. Faure, G. Guinet, R. Durand, Preparation of Monocrystalline Pt Microelectrodes and Electrochemical Study of the Plane Surfaces Cut in the Direction of the (111) and (110) Planes, J.Electroanal.Chem. 107 (1980) 205–209. https://doi.org/10.1016/S0022-0728(79)80022-4.

[26] M. Lukaczynska, E.A. Mernissi Cherigui, A. Ceglia, K. Van Den Bergh, J. De Strycker, H. Terryn, J. Ustarroz, Influence of water content and applied potential on the electrodeposition of Ni coatings from deep eutectic solvents, Electrochim. Acta. 319 (2019) 690–704. https://doi.org/https://doi.org/10.1016/j.electacta.2019.06.161.

[27] P. Sebastian, M. Tułodziecki, M.P. Bernicola, V. Climent, E. Gómez, Y. Shao-

Horn, J.M. Feliu, Use of CO as a Cleaning Tool of Highly Active Surfaces in Contact with Ionic Liquids: Ni Deposition on Pt(111) Surfaces in IL, ACS Appl. Energy Mater. 1 (2018) 4617–4625. https://doi.org/10.1021/acsaem.8b00776.

[28] M.C. Biesinger, L.W.M. Lau, A.R. Gerson, R.S.C. Smart, Resolving surface chemical states in XPS analysis of first row transition metals, oxides and hydroxides: Sc, Ti, V, Cu and Zn, Appl. Surf. Sci. 257 (2010) 887–898. https://doi.org/10.1016/j.apsusc.2010.07.086.

[29] M. Jana, P. Sivakumar, M. Kota, M.G. Jung, H.S. Park, Phase- and interlayer spacing-controlled cobalt hydroxides for high performance asymmetric supercapacitor applications, J. Power Sources. 422 (2019) 9–17. https://doi.org/10.1016/j.jpowsour.2019.03.019.

[30] P.F. Liu, S. Yang, L.R. Zheng, B. Zhang, H.G. Yang, Electrochemical etching of α-cobalt hydroxide for improvement of oxygen evolution reaction, J. Mater. Chem. A. 4 (2016) 9578–9584. https://doi.org/10.1039/c6ta04078k.

[31] T. Xue, X. Wang, J.M. Lee, Dual-template synthesis of Co(OH) 2 with mesoporous nanowire structure and its application in supercapacitor, J. Power Sources. 201 (2012) 382–386. https://doi.org/10.1016/j.jpowsour.2011.10.138.

[32] J.K. Chang, C.M. Wu, I.W. Sun, Nano-architectured Co(OH)2 electrodes constructed using an easily-manipulated electrochemical protocol for high-performance energy storage applications, J. Mater. Chem. 20 (2010) 3729–3735. https://doi.org/10.1039/b925176f.

[33] L.G. Shaidarova, A. V. Gedmina, G.K. Budnikov, Voltammetry of a Benzoquinone-Hydroquinone Redox Couple at Electrodes Modified with a Polyvinylpyridine Film Doped with Cobalt Phthalocyanine, J. Anal. Chem. 58

(2003) 171–175. https://doi.org/10.1023/A:1022366307246.

[34] P.S. Guin, S. Das, P.C. Mandal, Electrochemical Reduction of Quinones in Different Media: A Review, Int. J. Electrochem. 2011 (2011) 1–22. https://doi.org/10.4061/2011/816202.

[35] V. Vijaikanth, G. Li, T.W. Swaddle, Kinetics of reduction of aqueous hexaammineruthenium(III) ion at Pt and Au microelectrodes: Electrolyte, temperature, and pressure effects, Inorg. Chem. 52 (2013) 2757–2768. https://doi.org/10.1021/ic400062b.

[36] Y. Wang, J.G. Limon-Petersen, R.G. Compton, Measurement of the diffusion coefficients of [Ru(NH3) 6]3+ and [Ru(NH3)6]2+ in aqueous solution using microelectrode double potential step chronoamperometry, J. Electroanal. Chem. 652 (2011) 13–17. https://doi.org/10.1016/j.jelechem.2010.12.011.

[37] G. Pramanik, J. Humpolickova, J. Valenta, P. Kundu, S. Bals, P. Bour, M. Dracinsky, P. Cigler, Gold nanoclusters with bright near-infrared photoluminescence, Nanoscale. 10 (2018) 3792–3798. https://doi.org/10.1039/c7nr06050e.

[38] S. Caporali, F. Muniz-Miranda, A. Pedone, M. Muniz-Miranda, SERS, XPS and DFT study of xanthine adsorbed on citrate-stabilized gold nanoparticles, Sensors (Switzerland). 19 (2019) 1–10. https://doi.org/10.3390/s19122700.

[39] J. Hernández, J. Solla-Gullón, E. Herrero, Gold nanoparticles synthesized in a water-in-oil microemulsion: electrochemical characterization and effect of the surface structure on the oxygen reduction reaction, J. Electroanal. Chem. 574 (2004) 185–196. https://doi.org/https://doi.org/10.1016/j.jelechem.2003.10.039.

[40] J. Hernández, J. Solla-Gullón, E. Herrero, A. Aldaz, J.M. Feliu, Characterization of the Surface Structure of Gold Nanoparticles and Nanorods Using Structure Sensitive Reactions, J. Phys. Chem. B. 109 (2005) 12651–12654. https://doi.org/10.1021/jp0521609.

[41] J. Hernández, J. Solla-Gullón, E. Herrero, A. Aldaz, J.M. Feliu, Electrochemistry of Shape-Controlled Catalysts: Oxygen Reduction Reaction on Cubic Gold Nanoparticles, J. Phys. Chem. C. 111 (2007) 14078–14083. https://doi.org/10.1021/jp0749726.

[42] E. Herrero, L.J. Buller, H.D. Abruña, Underpotential Deposition at Single Crystal Surfaces of Au, Pt, Ag and Other Materials, Chem. Rev. 101 (2001) 1897–1930. https://doi.org/10.1021/cr9600363.

[43] S. Trasatti, O.A. Petrii, Real surface area measurements in electrochemistry, J. Electroanal. Chem. 327 (1992) 353–376. https://doi.org/10.1016/0926-860X(96)80148-7.